10.2514/6.2014-0491

AIAA SciTech Forum
13-17 January 2014, National Harbor, Maryland
55th AIAA/ASME/ASCE/AHS/ASC Structures, Structural Dynamics, and Materials Conference

Inclusion of Shear Effects, Tension, and Damping in a DTF Beam Model for Cable Modeling

Kaitlin S. Spak[1]
Virginia Polytechnic Institute and State University, Blacksburg, VA 24060

Gregory S. Agnes[2]
Jet Propulsion Laboratory, California Institute of Technology, Pasadena, CA 91011

and

Daniel J. Inman[3]
University of Michigan, Ann Arbor, 48109

The distributed transfer function method is applied to equations of motion for a space flight cable in an ongoing effort to characterize the effects of adding cabling to space structures. A cable model is presented in which the cable is modeled as a shear beam with multiple boundary constraints. Tension in the cable is included and a variety of damping mechanisms are incorporated. Comparison of the model results to experimental data is included, showing that the distributed transfer function cable model with equivalent cable property inputs can bound the range of cable responses and that hysteretic and connection stiffness damping improve the comparison between the model and experimental data.

Nomenclature

A	=	area of cable cross-section
c_v	=	damping coefficient for motion-based viscous damping
c_s	=	transverse damping coefficient for spring connection
$c_{s\theta}$	=	rotational damping coefficient for spring connection
E	=	composite elastic modulus of the cable
EI	=	bending stiffness of the cable
$F(s)$	=	transfer function matrix
G	=	shear modulus
$G(s)$	=	Laplace transform of the GHM damping expression as a function of s
I	=	area moment of inertia
k	=	connection spring stiffness
k_θ	=	connection spring rotational stiffness
l_i	=	cable section length
M	=	left side boundary condition matrix
N	=	right side boundary condition matrix
q	=	applied external force
s	=	Laplace transform variable
T	=	axial tension of the cable
T_m	=	transition matrix
w	=	cable displacement
$W(x,s)$	=	Laplace transform of the lateral cable displacement
α_D	=	GHM damping parameter, numerator
β	=	shear angle

[1] PhD Candidate, Mechanical Engineering Dept., 105 N. Wilson #102, Pasadena, CA 91106, AIAA Student Member.
[2] R&D Engineer, 355L, 126-107, AIAA Associate Fellow.
[3] Department Chair, Aerospace Engineering Dept., 3064 FXB, AIAA Fellow.

β_D = GHM damping parameter, denominator
γ_D = GHM damping parameter, numerator
δ_D = GHM damping parameter, denominator
$\eta(x,s)$ = solution vector for the distributed transfer function method
κ = shear factor
ρ = cable density
φ = total rotation angle
ψ = Laplace transform of the cable rotation

I. Introduction

CABLES have a wide variety of uses, from small cables for power and signal transmission to large wire ropes that serve as structural anchors for buildings and bridges. As structural analysis has become more precise, the behavior of cables has been studied more extensively; goals for these investigations include attempts to determine the contact forces between individual wires within a cable, determining stresses in the cable as a whole, and analyzing the vibration response. More precise cable models allow for more accurate prediction of failure, resonance, and performance.

In this case, the authors are interested specifically in the dynamic response of cables used on space flight structures, although the models presented would be applicable to any cable that could be described with effective beam properties. By modeling the cable as a beam, the bending stiffness of the cable can be taken into account and the vibration response can be determined without calculating friction forces between individual wires, which is difficult and computationally intensive. This paper presents a cable model developed from a beam-like equation of motion in which the cable properties are smeared to create effectively homogenous properties for the beam model. The distributed transfer function method is used as the solution method because it is an exact method, is well-suited to the repeating nature of cables attached to structures at multiple points, and can incorporate non-standard boundary conditions such as damped spring attachment points.

II. Background

Cables are like beams in that they have a reasonably constant cross-sectional area that is small compared to the length. While fine electrical cables may seem to be string-like, their bending stiffness is actually not negligible and must be considered for accurate vibration results. A beam model can also account for tension and damping in the cable. Thus, the overall structure of the cable is suited to modeling with a beam model; this has been verified by Castello and Matt [1]. Work from the Air Force Research Laboratory confirmed this and further showed that inclusion of shear effects was necessary for accurate cable modeling [2]. Using a beam model to characterize cable behavior works best for low-amplitude vibration modeling with minimal curvature so that internal friction forces due to wire slippage are minimized, or at least constant [3].

The space flight cables of interest are about 1 meter long and range in outer diameter from 7 mm to 22 mm. Although these cables seem to belong in the Euler-Bernoulli beam category due to its ratio of length to area, cables of this type must be modeled as shear beams [2]. This is due in part to the composite nature of the cable; the viscoelastic jacketing undergoes shear deformation and plane sections in the cable do not remain plane as the cable bends. Previous study showed that the Timoshenko beam model provided negligible additional accuracy for increased complexity, so all sources agree that the shear beam is the most applicable for cable modeling [4].

Until now, cable modeling has relied extensively on testing for results. Cable modeling is particularly difficult because of variations in cable construction and attachment points, leading to varying results for a single cable. Even cables of the same type show a large variation in their natural frequency response. It is unrealistic to aim for a model that can pinpoint the exact natural frequency and damping ratio for any given cable because of the inherent response variation; therefore, a cable model that bounds the span of the natural frequency responses is the goal for this work.

The distributed transfer function (DTF) method was developed by Yang and Tan for 1D elastic Euler Bernoulli beams [5]. The DTF method was extended for use in laminated beams, but shear and rotary inertia effects were still neglected [6]. To use the distributed transfer function method, the Laplace transform of the equation of motion is used to populate a matrix *F(s)* that can be manipulated to give information about the dynamic response of the system.

The ultimate goal of this research is to use the DTF method to create a cable model that can be added to structural models to quantify the changes in a structure's dynamic response due to the addition of cable harnesses.

The short term goal and scope of this paper is to model the cables themselves in order to predict their natural frequencies.

III. Model Development

To develop the cable model, we begin with a cable element undergoing both bending and shear as shown in Figure 1. Unlike an Euler-Bernoulli beam, in which plane sections remain plane, the cable is made up of individual wires that have a viscoelastic insulation layer which undergoes shear, so a shear beam is a more appropriate model to use. The cables for this model are assumed to have an overwrap or outer jacket which keeps the individual wires in the same basic configuration and maintains radial tension on the cable. As the cable bends, the wires move against each other, which alters the stiffness of the cable as a whole and is taken into account through careful calculation of the bending stiffness as a function of curvature and wire geometry, including number and arrangement of wires and lay angle.

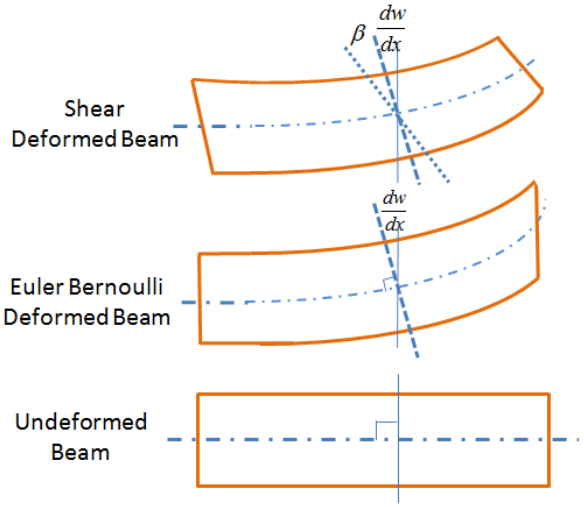

Fig. 1 Comparison of Euler Bernoulli and shear beam elements; cables experience shear deformation during bending and must be modeled as a shear beam.

Although there are three terms identifying the bending angles, only two are independent, yielding the relationship

$$\beta = \frac{\partial w}{\partial x} - \varphi \tag{1}$$

where β is the shear angle, dw/dx is the angle due to the Euler-Bernoulli bending of the beam, and φ is the total beam angle due to both bending and shear.

The governing equation for the shear beam cable model starts with a summation of the forces and moments on the cable element where $V(x,t)$ is the shear force acting on the element, $M_o(x,t)$ is the moment, and $q(t,x)$ is any applied external force.

$$\rho A\ddot{w}(x,t) = -V(x,t)' + q(x,t) \tag{2}$$

$$M_o(x,t)' + V(x,t) = 0 \tag{3}$$

From this starting point, we investigate an undamped model with tension and shear effects and then examine various damping mechanisms that can be included.

A. Undamped Cable Model

For an undamped shear beam [7],

$$V(x,t) = \kappa AG(\psi(x,t) - w(x,t)') \tag{4}$$

$$M_o(x,t) = EI\psi(x,t)' \tag{5}$$

These expressions are substituted into Eqs. (2) and (3) and then the two resulting equations are combined into one to yield the governing equation of motion for a shear beam in tension, Eq. (6),

$$\rho A\ddot{w} - \frac{EI\rho}{\kappa G}\ddot{w}'' + EIw'''' + Tw'' = q - \frac{EIq''}{\kappa AG} \tag{6}$$

where the cable parameters are density ρ, area A, bending stiffness EI, shear modulus G and shear factor κ, and tension in the cable is T.

To use the distributed transfer function method, Eq. (6) is transformed into the Laplace domain and rearranged so that the highest derivative is set equal to the other terms. For the undamped case of the shear cable in tension, this results in the equation

$$W'''' = -\frac{\rho A}{EI}s^2W + \left(\frac{\rho}{\kappa G}s^2 - \frac{T}{EI}\right)W'' + \frac{Q}{EI} - \frac{1}{\kappa AG}Q'' \tag{7}$$

This transformed equation of motion is now equivalent to the form

$$\frac{\partial}{\partial x}\eta(x,s) = F(s)\eta(x,s) + Q(x,s) \tag{8}$$

where $\eta(x,s)$ is the Laplace transform of the solution vector and $F(s)$ is the fundamental matrix for the system in which system properties are incorporated. For the undamped case with shear effects and tension, the fundamental matrix is

$$F_{Undamped} = \begin{bmatrix} 0 & 1 & 0 & 0 \\ 0 & 0 & 1 & 0 \\ 0 & 0 & 0 & 1 \\ -\frac{\rho A}{EI}s^2 & 0 & \frac{\rho}{\kappa G}s^2 - \frac{T}{EI} & 0 \end{bmatrix} \tag{9}$$

This matrix has two non-zero second order terms in the bottom row; in contrast, the Euler-Bernoulli formulation has only one term for an untensioned beam and the Timoshenko formulation has two terms, but the two terms contain fourth order and second order polynomial expressions in s, leading to greater complexity. As previous studies have shown that the additional complexity of the Timoshenko model does not lead to much greater accuracy, but significantly increases computation time, the shear beam model is considered sufficient. Tension is included because slack cables with zero tension have extreme non-linearities in their behavior, so lightly tensioned cables were tested to reduce these non-linearities and the model needed to reflect the test reality.

Once the fundamental matrix is determined, the incorporation of the system constraints are the next step. Figure 2 shows the cable as a beam, mounted to a test fixture at several points using a common method of attachment in which the cable is cable-tied to a TC105 mounting tab, as shown in Fig. 3. According to a previous study, accurate representation of the connection between a cable and host structure could not be modeled with pinned or fixed boundary conditions, and a spring model was used for the connection points [8]. For this DTF model, both translational and rotational spring and damper models were used to characterize the TC105 connection tabs. Experiments were conducted to determine the spring and damping coefficient inputs for the model.

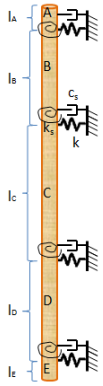

Fig. 2 Equivalent model for cable test set up. Fig. 3 Typical cable attachment point with cable tie fastened to TC105 tab.

To model the cable with multiple spring-damper attachment points, the unbranched distributed transfer function method was used, as modified from [9] to apply to a shear beam. For this case, the cable sections A, B, C, D and E are serially connected, so the fundamental matrix for each section is connected through the use of a transition

matrix. Since the four mounting points are identical, the transition matrix is the same for each section connection. The transition matrix fulfills the continuity requirement for the solution vector in which the solution on the left side of a connection point must be equal to the solution vector on the right side of the same point. If the bending stiffness is different for the different sections, the transition matrix takes the stiffness ratio into account, but since the cable is assumed to be homogenous along the length, the transition matrix has ratios of one along the diagonal. The attachment point is incorporated through the displacement and rotation terms of the solution vector. Thus, the transition matrix T_m for each connection point for this model is found through Eq. (9) and given by Eq. (10). Previous studies modeled the attachment with either a single linear spring, or a set of 3 linear springs to provide translational stiffness in each direction. To the best of the authors' knowledge, this is the first cable model that incorporates transverse connection damping and rotational connection stiffness and damping.

$$\eta(x,s)_- = T_m * \eta(x,s)_+ \tag{9}$$

$$T_m = \begin{bmatrix} 1 & 0 & 0 & 0 \\ 0 & 1 & 0 & 0 \\ 0 & \dfrac{k_\theta + c_{s_\theta} * s}{EI} & 1 & 0 \\ \dfrac{-k - c_s * s}{EI} & 0 & 0 & 1 \end{bmatrix} \tag{10}$$

The natural frequencies are determined by solving the eigenvalue problem for the entire system; the eigenvalues of the system are the roots of the characteristic equation

$$\det[M(s) + N(s) * \aleph_i] = 0 \tag{11}$$

where the determinant is a symbolic expression containing *s*, which can be solved for through symbolic computer coding or numerical methods. Matrices *M* and *N* represent the boundary conditions; in this case, for the free end conditions, the boundary condition matrices are

$$M = \begin{bmatrix} 0 & 0 & EI & 0 \\ 0 & 0 & 0 & -EI \\ 0 & 0 & 0 & 0 \\ 0 & 0 & 0 & 0 \end{bmatrix}, \qquad N = \begin{bmatrix} 0 & 0 & 0 & 0 \\ 0 & 0 & 0 & 0 \\ 0 & 0 & EI & 0 \\ 0 & 0 & 0 & -EI \end{bmatrix} \tag{12}$$

The fundamental matrix with connection points included is given as

$$\aleph_i = e^{F_i(s)(x - x_{i-1})} * T_{m_{i-1}} * e^{F_{i-1}(s)(l_{i-1})} \ldots * T_{m_1} * e^{F_1(s)(l_1)} \tag{13}$$

and for this specific cable model with five cable sections and four springs, the matrix used to determine the natural frequencies is

$$\aleph = e^{F(s)(l_E)} * T_m * e^{F(s)(l_D)} * T_m * e^{F(s)(l_C)} * T_m * e^{F(s)(l_B)} * T_m * e^{F(s)(l_A)} \tag{14}$$

The roots are of the form $s = j\omega_k, j = \sqrt{-1}, k = 1,2, \ldots$, where $\omega_k$is the *k*th natural frequency of the system. Solutions were obtained numerically; values of *s* were substituted into the characteristic equation and the determinant was evaluated. The minimums obtained from this process provide the natural frequencies, and can be solved to greater accuracy if desired. Mode shapes for the system are determined by substituting the natural frequency values for *s* back into the characteristic equation to solve for the displacement values (η) and then putting them into the solution equation

$$\eta(x,s) = \exp(F(s) * x) * \eta(0,s), \quad 0 \le x \le L \tag{15}$$

to get a function of *x* for each *s* value.

B. Damped Cable Models

The cable model that takes shear effects and tension into account has been introduced and can now be appended to include damping as well. Damping terms can be included as shear forces, or as additional terms acting on derivatives of the beam's response, or even as a variable bending stiffness term [3]. The simplest damping mechanism to include is viscous damping, sometimes known as motion based damping, in which the damping is

directly proportional to the rate of change of the beam velocity or its rotation. Beam models with viscous damping are common, and are included here not as a novel concept, but to present the full range of damping mechanisms and show how they appear in the final DTF model in comparison to the hysteretic model.

A viscous damping term is added to Eqs. (2) and (3), and the equations are combined as previously to yield a new, viscously damped equation of motion and fundamental matrix.

$$\rho A\ddot{w} - \frac{EI\rho}{\kappa G}\ddot{w}'' + EIw'''' + Tw'' - \frac{EIc_v}{\kappa AG}\dot{w}'' + c_v\dot{w} = q - \frac{EIq''}{\kappa AG} \tag{16}$$

$$F_{Viscous} = \begin{bmatrix} 0 & 1 & 0 & 0 \\ 0 & 0 & 1 & 0 \\ 0 & 0 & 0 & 1 \\ -\frac{\rho A}{EI}s^2 - \frac{c_v}{EI}s & 0 & \frac{\rho}{\kappa G}s^2 - \frac{T}{EI} + \frac{c_v}{\kappa AG}s & 0 \end{bmatrix} \tag{17}$$

A more sophisticated type of damping that deals with internal friction is hysteretic damping [10]. For hysteretic damping, the initial starting equations are the same, as is the equation for shear, but for a viscoelastic material, stress is

$$\sigma(x,t) = E\epsilon(x,t) - \int_0^t g(t-\tau)\epsilon(x,t)ds \tag{18}$$

So the moment becomes

$$M_o = EI\psi(x,t)' - \int_0^t g(t-\tau)w(x,t)''ds \tag{19}$$

Using the form in which hysteresis is applied to w, substitution of Eq. (19) into Eqs. (2) and (3) yields

$$\rho A\ddot{w}(t,x) = -\kappa AG\psi(t,x)' + \kappa AGw(t,x)'' + q(t,x) \tag{20}$$

$$EI\psi(t,x)'' + \int_0^t g(t-\tau)w(t,x)'''dt - \kappa AG\psi(t,x) + \kappa AGw(t,x)' = 0 \tag{21}$$

The tension term is added, as well as the viscous damping terms.

$$\rho A\ddot{w}(t,x) = -\kappa AG\psi'(t,x) + \kappa AGw''(t,x) + c_v\dot{w} + q(t,x) \tag{22}$$

$$EI\psi''(t,x) + Tw' + \int_0^t g(t-\tau)w'''dt - \kappa AG\psi(t,x) + \kappa AGw'(t,x) = 0 \tag{23}$$

Eqs. (22) and (23) are combined into a single equation to eliminate the rotation variable.

$$\rho A\ddot{w} - \frac{EI\rho}{\kappa G}\ddot{w}'' + EIw'''' + \frac{EIc_v}{\kappa AG}\dot{w}'' - \int_0^t g(t-\tau)w''''dt + c_v\dot{w} + Tw'' = q - \frac{EIq''}{\kappa AG} \tag{24}$$

Again, the Laplace transform is taken and the equation is rearranged to match the form in which the highest derivative is set equal to the other terms.

$$\rho AWs^2 - \frac{EI\rho}{\kappa G}W''s^2 + EIW'''' + \frac{EIc_v}{\kappa AG}W''s - \frac{1}{s}G(s)W'''' + c_vWs + TW'' = Q - \frac{EIQ''}{\kappa AG} \tag{25}$$

$$W'''' = \frac{-(\rho As^2 + c_vs)W + \left(\frac{EI\rho}{\kappa G}s^2 - \frac{EIc_v}{\kappa AG}s - T\right)W'' + Q - \frac{EIQ''}{\kappa AG}}{\left(EI - \frac{1}{s}G(s)\right)} \tag{26}$$

This fulfills the requirement for the state space equation and we can determine that the hysteretically damped fundamental matrix is:

$$F_{Hysteretic} = \begin{bmatrix} 0 & 1 & 0 & 0 \\ 0 & 0 & 1 & 0 \\ 0 & 0 & 0 & 1 \\ \frac{-\rho As^2 - c_vs}{EI - \frac{1}{s}G(s)} & 0 & \frac{\frac{EI\rho}{\kappa G}s^2 - \frac{EIc_v}{\kappa AG}s - T}{EI - \frac{1}{s}G(s)} & 0 \end{bmatrix} \tag{27}$$

The hysteretic damping term *G(s)* was included in the form given by [11] for viscoelastic materials.

$$G(s) = \frac{\alpha_D s^2 + \gamma_D s}{s^2 + \beta_D s + \delta_D} \tag{28}$$

It is clear that the various damping terms add complexity in varying degrees; terms that add an entire term to the damping matrix (i.e. terms multiplying W' and W''') will slow down computation time considerably. Another consideration is the complexity of the symbolic *s* term; higher orders of *s* make for more difficult calculation of the determinant in the solution step. This can be avoided by using a numeric solution, but the accuracy of the natural frequency calculation is then dependent on the step size of the numerical method.

IV. Model Parameters

The models presented are applicable for any shear beam that may experience damping or tension. However, to use these models for cables specifically, the model inputs ρ, *A*, *EI*, and *G* must be determined to describe the cable. Because the model assumes a homogenous cross section, these parameters must be calculated to be equivalent to the cable as a whole. Cable parameters are generally found by performing dynamic tests and backing out the beam parameters from the dynamic tests. However, since one of the goals of this project is the ability to calculate cable frequency bounds a priori, with no dynamic experimental testing, the authors have determined equivalent cable properties based on the geometry and component materials of the cables [12]. Four types of cable were modeled and subsequently tested: single-stranded cables in 1X7, 1X19, and 1X48 configurations, and a multi-stranded cable made up of seven 1X7 strands, known as a 7X7 cable. The mass, length, outer diameter, and lay angle were measured for each of the five experimental samples of each type of cable and averaged. These cable measurements were used for property calculations as described in [12] and are listed in Table 1.

Table 1 Average measured values for each cable type

	1X7 Cable	1X19 Cable	1X48 Cable	7X7 Cable
Number of Wires	7	19	48	49
Mass (kg)	0.0708	0.1905	0.4481	0.4944
Length (m)	0.7692	0.7782	0.7744	0.7744
Outer Diameter (m)	0.0074	0.0127	0.0204	0.0216
Lay Angle (deg)	19.6	16.5	18.4	17.4
Lay Angle (rad)	0.3417	0.2873	0.3217	0.3037

The equivalent cable properties were determined through a combination of cable measurement and weighted average of the material properties of the constituent materials making up the cable; since the rule of mixtures was used for the density and the moduli values, and area could be calculated using either overall area or individual wire area, the cable properties span a range. Lower and upper limits based on uncertainty and alternative methods in the measurements yield a range of input values rather than a single value for each property. These upper and lower limits are the maximum and minimum property parameters used in the model, presented in Table 2. All cables were under 8.89 N of tension during testing, so all model trials used *T = 8.89.*

Table 2 Calculated cable properties used as model inputs for each cable type

	1X7 Cable		1X19 Cable		1X48 Cable		7X7 Cable	
Calculated Cable Property	Value for Min Frequency	Value for Max Frequency	Value for Min Frequency	Value for Max Frequency	Value for Min Frequency	Value for Max Frequency	Value for Min Frequency	Value for Max Frequency
ρA (kg/m)	0.145	0.060	0.425	0.245	0.969	0.345	1.23	0.347
EI (kg-m^3/s^2)	3.02	3.65	21.8	26.3	168.4	203.4	101.8	187.7
κAG (kg-m/s^2)	4.21E+05	2.75E+05	1.23E+06	7.48E+05	3.16E+06	1.89E+06	3.55E+06	1.93E+06

V. Experimental Testing

To collect experimental data, five samples were acquired for each of four types of typical spaceflight cable for a total of 20 cable samples. Figure 4 shows the three types of single-stranded cables and one multi-stranded cable that were investigated. In Fig. 4, the blue rings indicate 1X7 cable strands to show the difference between single stranded cables, in which each successive layer is a concentric ring of individual wires around the previous layer, and multi-stranded cables, in which strands make up the layers. All cable samples were made of MIL 27500-TG2T14 wires, contra-helically twisted and machine wrapped with Kapton. Cables were excited with a shaker producing white noise at $0.1g$ to $0.4g$ and the response was measured at the driving point with a non-contact laser vibrometer. Each cable sample was tested at least 15 times. Due to the flight cables' inherent differences in wire alignment, wire friction, and attachment, the experimental natural frequency results have variation, spanning a range of values for each mode, which is what the model is designed to capture by running both upper and lower bound property values. The range of experimental frequencies for each mode was recorded, as well as the average natural frequency for the first four modes; these details can be found in Table 5 in the Appendix. Experimental testing is discussed in further detail in [13].

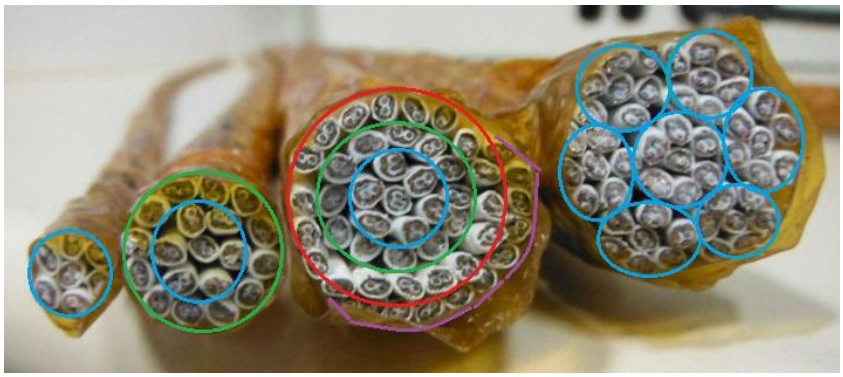

Fig. 4 Four types of cable investigated; 1X7, 1X19 and 1X48 single stranded cables and 7X7 multi-stranded cable.

VI. Results

To show the value of the model, the natural frequency and damping results are compared to experimental data. As listed in Table 2, the minimum frequency bound occurs when the ρA term is a maximum, the bending stiffness term EI is a minimum, and the shear term depends on the maximum area. The maximum frequency bound occurs when the ρA term is a minimum, the bending stiffness term is a maximum, and the shear term depends on the minimum area. Improved property calculation will result in a narrower range for the property values. The goal is to have the modeled natural frequency range (determined with parameters calculated only from basic cable measurements) just cover the range of frequencies shown by flight cables.

Six model trials were run for each cable; an undamped case, a viscously damped case, and a hysteretically damped case were each run with the parameter inputs for the minimum frequency, and then run again with the parameter inputs for the maximum frequency. This gave the range for the first four modes for the undamped, viscously damped, and hysteretically damped cases, which were then compared to the experimentally determined ranges. Models were run with the fundamental matrices developed in Section III, with connection parameters and damping parameters listed in Table 3.

Table 3 Connection and damping inputs

	Connection Parameters				Hysteretic Damping Coefficients			
Cable Type	Connection Stiffness, k, N/m	Rotational Connection Stiffness, k_θ, N-m/rad	Connection Damping, c_s, kg/s	Viscous Damping Coefficient, c_v, kg/s	α_D	β_D	γ_D	δ_D
1X7	1.50E+03	1.97	0.5	2	5	56.6	283	80089
1X19	1.50E+04	1.769	2	10	100	87.6	8760	191844
1X48	1.00E+05	2.385	10	20	1000	161.4	161400	651249
7X7	5.00E+04	2.385	8	20	1000	106	106000	280900

Connection stiffness and rotational connection stiffness applies to all of the model trials. The viscous damping trials used only the viscous damping coefficient, and the hysteretic damping trials used the hysteretic damping coefficients and connection damping. Damping coefficients correspond to a damping ratio of about 0.01 for connection damping for all cables and 0.05 for viscous damping.

Table 4 shows the results for the three model cases and experimental data for the first mode for each cable. The model certainly bounded the experimental frequency for each cable for the first mode. However, the model tends to predict a much wider frequency range than is observed experimentally, so further refinement of the model is necessary. Since the absolute maximum and minimum input values were used, the next step is to determine where those absolute values can be restricted to reduce the predicted frequency range.

Table 4 First mode experimental range and average frequencies and model frequency range for each cable

	1X7 Cable		1X19 Cable		1X48 Cable		7X7 Cable	
	Min (rad)	Max (rad)	Min (rad)	Max (rad)	Min (rad)	Max (rad)	Min (rad)	Max (rad)
Experimental Range	253	334	420	481	754	838	498	585
Experimental Average	283		438		807		530	
Undamped	217	335	396	675	682	1131	442	830
Viscously Damped	218	341	399	688	685	1160	444	844
Hysteretically Damped	218	343	391	686	678	1165	438	845

With three exceptions out of the sixteen cases (first four modes for each of the four cable types), the hysteretically damped model was able to bound the experimental data frequency range. Figures 5, 6, 7 and 8 show the experimental and model results for the first four modes for the 1X7, 1X19, 1X48, and 7X7 cables, respectively. The experimental data and model results represented in these figures appear in tables in the Appendix, divided by damping type. The model is very dependent on the connection point stiffness, as is to be expected. Adding rotational stiffness to the connection point model (modeled through the transition matrix T_m) decreases the natural frequency result, as does adding translational connection damping. These are both aspects that build on past cable models, which do not generally take non-standard boundary conditions into account.

Figure 5 presents the model results for the smallest, most flexible cable. This cable model had the poorest results for the undamped model, but inclusion of hysteretic and connection damping was able to bound the experimental data for the third and fourth modes while viscous damping barely shifted the mode ranges. The lack of agreement for all models for the second mode is problematic, but previous studies agree that the smaller the cable, the more difficult it is to model as a beam, so this 7 mm cable may be toward the lower limit of what a beam model can accurately portray. The first mode, which is of greatest interest because it has the highest amplitude, was well modeled by the hysteretically damped model for the 1X7 case. It should again be noted that the cable parameters for this model were determined purely through physical cable measurement and calculation, not dynamic testing.

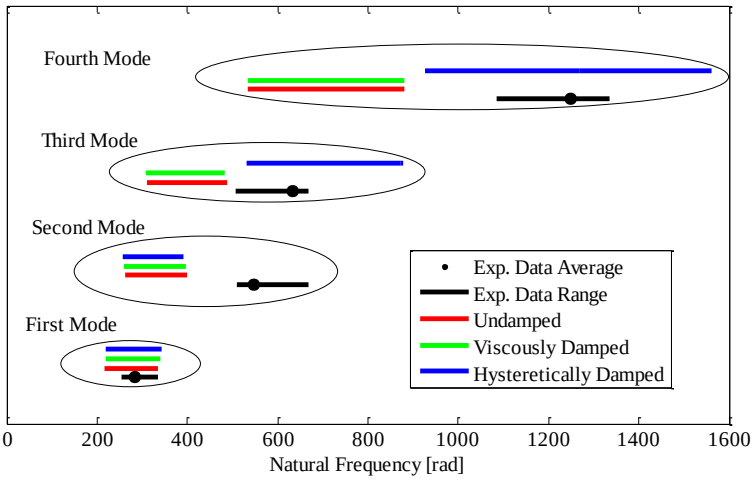

Fig. 5 Comparison of model results and experimental data for 1X7 cable

Figure 6 and Figure 7 show the results for the 1X19 cable with diameter of about 12 mm, and the 1X48 cable, with diameter of about 21 mm. These are typical mid-size and large spaceflight cables, and were modeled well as beams. These stiffer cables showed less experimental variation, likely due in part to less movement of the cable and thus less internal friction and inherent damping, which contributes to variation in response. Except for the fourth mode of the 1X48 cable, the model easily spanned the experimental frequency range, but again, the model range is too large to be really useful for model prediction. Further investigation of the maximum and minimum cable parameters are necessary to reduce this range to be more applicable for natural frequency prediction.

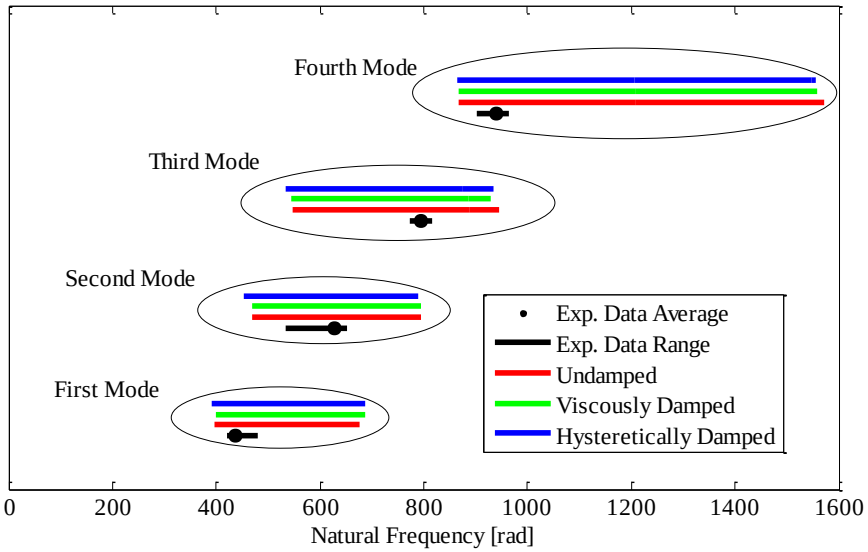

Fig. 6 Comparison of model results and experimental data for 1X19 cable

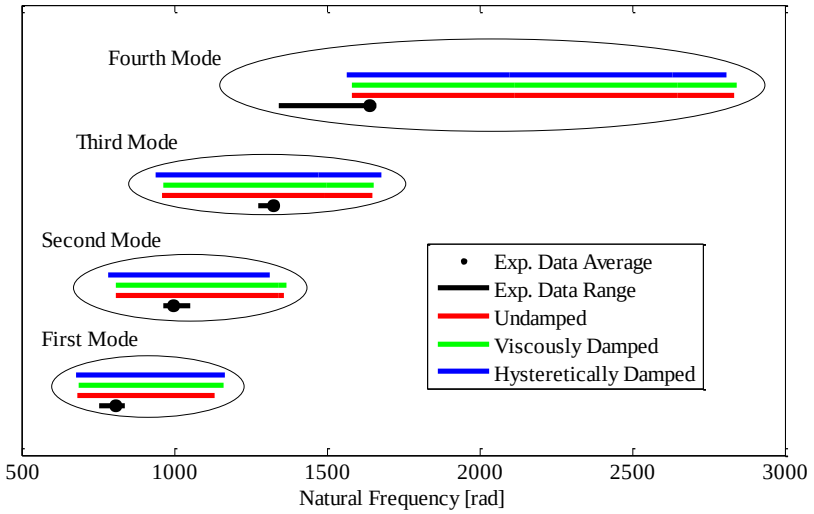

Fig. 7 Comparison of model results and experimental data for 1X48 cable

Figure 8 shows the comparison between experimental and model results for the 7X7 cable, a more flexible cable for its size due to multi-strand configuration. The lower bending stiffness and higher mass result in lower natural frequencies than the similarly sized 1X48 cable. Here again, as in the 1X7 cable, the hysteretic damping shifts the model range to more closely match the third and fourth mode experimental data. Range could still be reduced for greater accuracy in prediction, but first and second modes are completely bounded as desired, and the fourth mode is bounded by the hysteretically damped case.

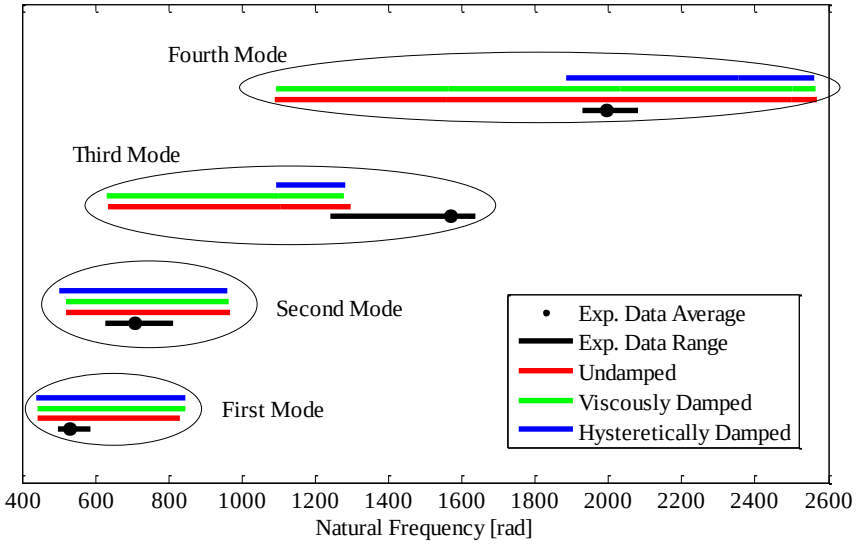

Fig. 8 Comparison of model results and experimental data for multi-stranded 7X7 cable

In most cases, even the undamped model agreed with the experimental data to some degree, but in a few cases (third and fourth modes of the 1X7 and 7X7 cables) the hysteretic model greatly increased agreement and/or decreased the range appropriately. Closer inspection of these cases showed that the hysteretic damping was eliminating one mode much more quickly than the other modes, as shown in Fig. 9, drastically changing the frequency response minimum and maximum for the higher modes. This shows that a more scientific approach to determine damping coefficients could lead to greater accuracy and reduced frequency ranges for the models.

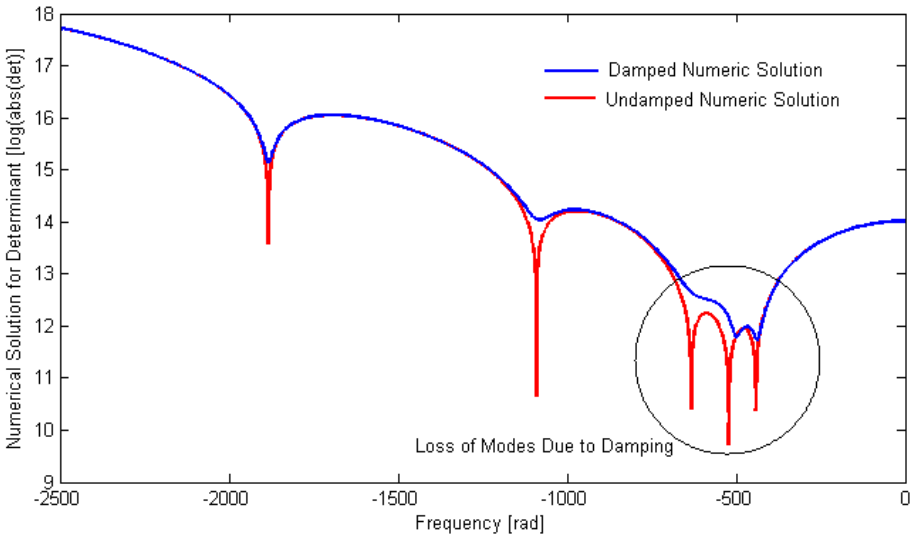

Fig. 9 Numerical solution for 7X7 cable showing mode elimination as damping increases

Overall, this distributed transfer function cable model is well on its way to being a useful tool. The inclusion of shear effects, tension, and damping was successful and extended the utility of the distributed transfer function model beyond the simple Euler-Bernoulli beam formulation. The hysteretically damped DTF cable model correctly bounded the natural frequency range for 13 of the 16 trials, for cables ranging in size from 7 mm diameter (7 wires) to 21 mm diameter (49 wires). The next steps will include determining if the cable parameters can be more narrowly bounded to reduce the range of predicted frequencies to a more useful result, and determining damping parameters to more accurately reflect the cable's physical damping and further reduce the natural frequency range.

VII. Conclusion

The presented model is a useful extension of the DTF method and can be applied to any beam-like system for which equivalent homogenous parameters can be determined. Adding shear effects, tension, and damping to the standard Euler-Bernoulli DTF method adds complexity, but also increases the utility of the model to predict behavior for more materials. Although the range of frequencies predicted is still fairly large, improved calculation of cable properties should reduce this spread and yield an average value that can be used for reliable predictions. In addition, the difference in experimental frequencies for two cables with identical size and wires but different wrapping process and lay direction shows that the cables themselves will have a range of frequencies for any given size and number of wires, so having a model to predict a range of frequencies may actually more useful for a wider variety of cable types. Eventually, these cable models will be integrated into structure models to investigate the damping effects of structures due to cable harnesses.

Appendix

Table 5 Experimental minimum, average, and maximum natural frequency values

	1X7 Cable			1X19 Cable			1X48 Cable			7X7 Cable		
	Min (rad)	Avg (rad)	Max (rad)	Min (rad)	Avg (rad)	Max (rad)	Min (rad)	Avg (rad)	Max (rad)	Min (rad)	Avg (rad)	Max (rad)
Mode 1	253	283	334	420	438	481	754	807	838	498	530	585
Mode 2	509	548	668	534	628	653	966	996	1054	626	707	813
Mode 3	508	632	668	773	795	816	1274	1325	1343	1241	1571	1638
Mode 4	1086	1249	1335	901	939	964	1343	1640	1663	1928	1995	2081

Table 6 Undamped shear beam model; no connection damping, no cable damping

	1X7 Cable		1X19 Cable		1X48 Cable		7X7 Cable	
	Min (rad)	Max (rad)	Min (rad)	Max (rad)	Min (rad)	Max (rad)	Min (rad)	Max (rad)
Mode 1	217	335	396	675	682	1131	442	830
Mode 2	261	399	470	794	810	1360	522	966
Mode 3	311	489	548	946	962	1650	633	1296
Mode 4	534	882	868	1571	1580	2835	1091	2570

Table 7 Damped shear beam model; viscous damping

	1X7 Cable, $c_v = 2$		1X19 Cable, $c_v = 10$		1X48 Cable, $c_v = 20$		7X7 Cable, $c_v = 20$	
	Min (rad)	Max (rad)	Min (rad)	Max (rad)	Min (rad)	Max (rad)	Min (rad)	Max (rad)
Mode 1	218	341	399	688	685	1160	444	844
Mode 2	260	397	470	794	810	1367	522	964
Mode 3	309	482	544	929	965	1655	632	1279
Mode 4	533	880	867	1558	1583	2843	1093	2564

Table 8 Damped shear beam model; connection damping and hysteretic damping

	1X7 Cable		1X19 Cable		1X48 Cable		7X7 Cable	
	Min (rad)	Max (rad)	Min (rad)	Max (rad)	Min (rad)	Max (rad)	Min (rad)	Max (rad)
Mode 1	218	343	391	686	678	1165	438	845
Mode 2	258	391	453	789	783	1315	501	962
Mode 3	531	877	533	934	941	1680	1094	1280
Mode 4	926	1560	864	1555	1565	2810	1886	2560

Acknowledgments

The first author thanks the NASA Space Technology Research Fellowship program for generous support and the San Gabriel Valley AIAA Chapter and Virginia Space Grant Consortium for additional funding. Space flight cables were provided at cost by Southern California Braiding, Co. The third author gratefully acknowledges the support of AFOSR Grant number FA9550-10-1-0427 monitored by Dr. David Stargel. This research was carried out at the Jet Propulsion Laboratory, California Institute of Technology, under a contract with the National Aeronautics and Space Administration.

References

[1]Castello D. A., and Matt C. F. T., "A Validation Metrics Based Model Calibration Applied on Stranded Cables," *Journal of the Brazilian Society of Mechanical Scientists and Engineers*, Vol. 33, No. 4, 2011, pp. 417–427.

[2]Goodding, J. C., Ardelean, E. V., Babuska, V., Robertson, L. M., and Lane, S. A., "Experimental Techniques and Structural Parameter Estimation Studies of Spacecraft Cables," *Journal of Spacecraft and Rockets*, Vol. 48, No. 6, 2011, pp. 942–957.

[3]Spak, K.S, Agnes, G.S, and Inman, D. J, 2013, "Cable Modeling and Internal Damping Developments", Applied Mechanics Reviews, Vol. 65, Issue 1, DOI:10.1115/1.4023489.

[4]Spak, K.S., Agnes, G.A., and Inman, D.J., "Comparison of Damping Models for Space Flight Cables," International Modal Analysis Conference, Garden Grove, CA, 2013, Paper #77.

[5]Yang B., and Tan C.A., "Transfer Functions of One-Dimensional Distributed Parameter Systems," *Journal of Applied Mechanics*, Vol. 59, Dec. 1992, pp. 1009-1014.

[6]Majeed, A.M., Al-Ajmi, M., and Benjeddou, A., "Semi-analytical Free-Vibration Analysis of Piezoelectric Adaptive Beams using the Distributed Transfer Function Approach," *Structural Control and Health Monitoring*, Vol. 18, 2011, pp. 723-736.

[7]Timoshenko, S., *Vibration Problems in Engineering*, 2nd ed., D. Van Nostrand Company, Inc, New York, 1937, pp. 337-338.

[8]Coombs, D. M., Goodding, J. C., Babuska, V., Ardelean E., Robertson L. M., and Lane S.A., "Dynamic Modeling and Experimental Validation of a Cable-Loaded Panel," *Journal of Spacecraft and Rockets*, Vol. 48, No. 6, 2011, pp. 958-973. doi: 10.2514/1.51021

[9]Yang, B., "Exact Transient Vibration of Stepped Bars, Shafts and Strings Carrying Lumped Masses," *Journal of Sound and Vibration*, Vol. 329, No. 8, 2010, pp. 1191-1207. doi: 10.1016/j.jsv.2009.10.035

[10]Banks, H.T., Fabiano, R.H., Wang, Y., Inman, D.J., and Cudney, H., "Spatial Versus Time Hysteresis in Damping Mechanisms," Proceedings of the 27th Conference on Decision and Control, Austin, Texas, 1988, pp 1674-1677.

[12]Friswell, M.I., Inman, D.J., and Lam, M.J., "On the Realisation of GHM Models in Viscoelasticity," *Journal of Intelligent Material Systems and Structures*, Vol. 8, No. 11, 1997, pp. 986-993.

[12]Spak, K.S., Agnes, G.A., and Inman, D.J., " Cable Parameters for Homogenous Cable-Beam Models for Space Structures," International Modal Analysis Conference, Orlando, FL, 2014, Paper #17.

[13]Spak, K.S., Agnes, G.S., and Inman, D.J. "Toward Modeling of Cable Harnessed Structures: Cable Damping Experiments", 54th AIAA/ASME/ASCE/AHS/ASC Structures, Structural Dynamics, and Materials Conference, Boston, MA, AIAA-2013-1889, April 2013.